Colloid Polym Sci 278:728–735 (2000)

ORIGINAL CONTRIBUTION

D. Vollmer

Phase separation in microemulsions: stepwise change of the droplet size

Received: 27 July 1999
Accepted: 4 January 2000

D. Vollmer
Institut für Physikalische Chemie,
Welder Weg 11, 55099 Mainz, Germany
e-mail: vollmerd@mail.uni-mainz.de
Tel.: +49-6131-3924050
Fax: +49-6131-3923768

Abstract The kinetics of phase separation is studied for a droplet-phase microemulsion, where the phase separation is induced by constant heating. In that case the droplets shrink in a stepwise manner at the expense of a growing water-rich phase. The parameter dependence of the height of the energy barrier preventing this phase separation is discussed, and a general argument for the stepwise decrease in the droplet size is presented, which provides a quantitative description of microcalorimetric data. Finally, a superimposed structure on the signal of the apparent specific heat is explained by an argument which underlines the importance of the conservation of volume and of interfacial area for the modeling of this explicitly time-dependent kinetics.

Key words Microemulsion · Calorimetry · Kinetics of phase transitions · Nucleation

Introduction

Surfactant mixtures show fascinating kinetics upon driving the system out of equilibrium. Typically, this is done by mechanical treatment, by a sudden change of composition, or by a temperature jump. The most intensively studied mechanically induced transition in surfactant mixtures is the formation of multilamellar vesicles (onions), which occurs on shearing a lamellar phase [1–4]. A sudden change of composition may lead to the formation of myelins [5–8]. These fingerlike structures occur when adding water (oil) onto a water (oil) swollen lamellar phase. Mechanical pinching of a cylindrical vesicle might lead to a pearling instability, where incompressible hydrodynamic flows in combination with the bending rigidity of the flow lead to disintegration of the cylinder into a row of equidistant monodisperse droplets. Finally, temperature-jump experiments have been performed to investigate the phase separation of a bicontinuous, sponge, lamellar, or droplet phase, respectively, into one or several coexisting phases with different morphologies [9–11].

During the last few years significant improvement has been made in the description of the kinetics observed in these experiments, i.e., the dependence of the pathway to the final state on the choice of the parameters and on the setup of the experiment; however, in a few cases [12] modeling of the kinetics starting from the equilibrium thermodynamic potentials and the transport coefficients could not be established. A major problem is that frequently not even the thermodynamic properties of the initial and final states are known. Although, some relevant parameters entering the equilibrium free energies have been identified during the last few years [13–20], in general, their precise values, as well as their temperature and composition dependencies are only roughly known.

In this article, we discuss an example where a quantitative description of nontrivial kinetics is possible. Driving a single phase (1Φ) of nanometer-sized water droplets embedded in an oil matrix into a two-phase (2Φ) region by applying a constant heating rate may lead to a stepwise decrease in the size of the droplets and a stepwise increase in the volume fraction of the water-rich phase [21–23]. A schematic visualization of this process

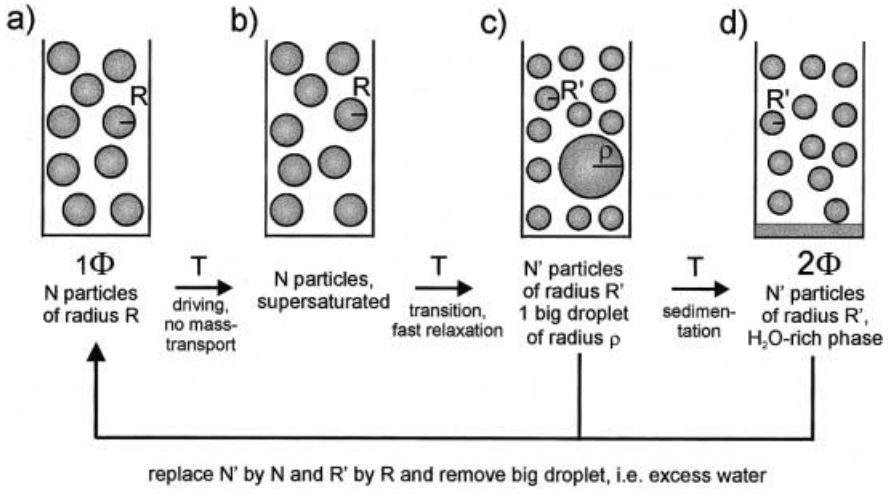

Fig. 1 Schematic drawing of the temperature-dependent microstructure of a mixture containing water droplets embedded in an oil matrix. Increasing temperature leads to the formation of a water-rich phase coexisting with smaller-sized water droplets. Under constant heating the size of the droplets decreases step wise. Single phase (1Φ), two-phase (2Φ)

is given in Fig. 1. The reduction in the size of the droplets is connected to a burst of nucleation of large water droplets feeding the coexisting water-rich phase. Since this stepwise change of the size of the droplets may lead to oscillations in the turbidity of the sample and its apparent specific heat, the temperature difference between subsequent bursts of nucleation is called the period of oscillations. We dubbed this phase separation cascade nucleation to emphasize the generalization of classical nucleation theory needed to describe this kinetics. The origin of cascade nucleation, the composition and the temperature dependence of the period, as well as the observation and the reason for a superimposed structure on the signal for the apparent specific heat are discussed in the following sections.

In the next section we give basic information about the experiments. Then, we discuss the height of the energy barrier preventing a decrease in the size of the droplets. This is followed by a description of the mechanism leading to cascade nucleation under constant heating. We then explain the reason for the temporal variation of the time lag between steps in the course of phase separation. Finally, the main results are summarized.

Experimental findings

Microemulsions

Water and oil are immiscible. A sample containing water and oil will phase separate into macroscopic water and oil domains, since the surface tension of the interface between water and oil tends to minimize the area of the interface. The interfacial tension between water and oil domains decreases by several orders of magnitude when surfactant molecules are added [17, 20, 24, 25]. These molecules have a water-soluble polar head group and an oil-soluble apolar tail separating the water and oil domains by a liquidlike monolayer of fixed average area per surfactant molecule [26]. In this case of very low interfacial tension, morphologies requiring a large interfacial area may be thermodynamically stable. If, furthermore, the mixture of water, oil, and surfactant is isotropic, transparent, and of low viscosity it is called a microemulsion [27, 28].

At present, the thermodynamic properties of microemulsions containing a strong non-ionic surfactant of the type of alkyl polyglycol C_iE_j are being investigated very carefully. The phase behavior has been extensively studied by Olsson and Wennerstöm [16], Kahlweit, Strey and coworkers [25, 28], and Vollmer et al. [31], and detailed knowledge of the temperature-dependent and composition-dependent morphology is available [16, 17, 26, 31, 32, 33].

Materials

In the present article we restrict ourselves to mixtures of water, octane (Merck, Darmstadt), and $C_{12}E_5$, i.e., $CH_3(CH_2)_{11}(OCH_2CH_2)_5OH$ (Nikko Chemicals, Tokyo, Japan). Sample compositions are given by the volume fraction of water, ϕ_w, octane, ϕ_o and surfactant, ϕ_s. The surfactant investigated has a low critical micellar concentration in water and octane, i.e., to a good approximation all surfactant molecules are located at the water–oil interface.

Droplet size

A section through the phase prism of the mixture is shown in Fig. 2 for a fixed volume ratio of octane and $C_{12}E_5$ and a varying volume fraction of water. Within the 1Φ region the size of the droplets is determined by the composition. Their average radius, $R_{1\Phi}$, can be calculated from the conservation laws of their volume, $4/3\pi NR_{1\Phi}^3 = V\phi_d \simeq V(\phi_w + 0.5\phi_s)$, and of their interfacial area, $4\pi NR_{1\Phi}^2 l_s = V\phi_s$, where N denotes the number of droplets within a volume element V, ϕ_d the volume fraction of droplets, and l_s the average length of a surfactant molecule [17, 32, 33].[1] This yields

$$R_{1\Phi} = \frac{3l_s\phi_d}{\phi_s} \quad . \tag{1}$$

The effective thickness of the surfactant monolayer is found to be $l_s \approx 1.3$ nm. The droplet radius is of the order of 2–20 nm, the total

[1] We define the volume of a water droplet to be the sum of the volume of enclosed water and of the hydrophilic part of the surfactant molecule. For mixtures of water, octane, and $C_{12}E_5$ the latter is roughly $\phi_s/2$

oil–water interfacial area is of the order of $100\,m^2$ and 10^{16}–10^{18} droplets are formed per cubic centimeter. Note that the radius $R_{1\Phi}$ does not depend on temperature.

In contrast, within the $\overline{2\Phi}$ region the radius R_{opt} of the droplets only depends on temperature and it is independent of composition [17]. For temperatures sufficiently below the size of the reverse micelles and several degrees above the phase-inversion temperature, $\bar{T} = 32.5\,^{\circ}C$, the optimum radius has been determined to be [18]

$$R_{opt}(T) \simeq \frac{1}{a\,(T-\bar{T})}\ , \qquad (2)$$

where $a = 1.2\ \times 10^{-3}\ K^{-1}\text{Å}^{-1}$.

The change in the size of the droplets under varying composition and temperature, is sketched in Fig. 2. The 1Φ and 2Φ regions are separated by a phase boundary denoted the water emulsification boundary (WEB). At the phase boundary both radii are equal, $R_{1\Phi} = R_{opt}$ [31, 34].

Due to conservation of the enclosed volume and of the total surface of all droplets, water droplets can only attain their optimum radius above the emulsification failure, where they are in equilibrium with the water-rich phase. This leads to a decrease in the WEB towards lower temperatures under increasing ϕ_w (Fig. 2).

Equilibrium free energy

The equilibrium phase behavior of the mixture has been described [31] by the bending free energy [35] of the interface between water and oil, with the additional constraint that the area of the interface and that of the enclosed volume are fixed by composition. Within a mean-field approximation the bending free energy of N monodisperse droplets is given by [22]

$$F_b = 8\pi R^2 N\kappa\left(\frac{1}{R} - \frac{1+\overline{\kappa}/(2\kappa)}{R_{opt}(T)}\right)^2 + 4\pi N\overline{\kappa}\ . \qquad (3)$$

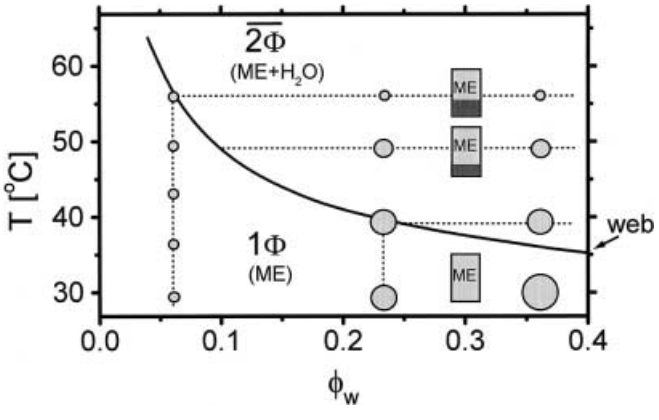

Fig. 2 Section through the phase prism for mixtures of water, octane, and $CH_3(CH_2)_{11}(OCH_2CH_2)_5OH$ for varying volume fraction of water and fixed volume ratio of octane and $C_{12}E_5$. The *solid line* shows the temperature dependence of the water emulsification boundary (WEB) for $\phi_o/\phi_s = 5.7$. The variation of the size of the *circles* shows the composition and temperature dependence of the size of the droplets. For temperatures below the WEB the mixture is a single phase, whereas a water-rich phase coexists with a droplet-phase microemulsion (*ME*) for temperatures above the WEB. The increase in the volume fraction of the water-rich phase with increasing temperature is indicated by the size of the *dark area* of the "test tubes". Due to the small size of the droplets the ME phase is transparent within the 1Φ as well as within the 2Φ region

The parameters κ and $\overline{\kappa}$ are the bending and the Gaussian modulus of the interface, respectively. R represents the radius of the droplets either in the 1Φ region or in the 2Φ region. For droplets the optimum radius corresponds to the curvature that minimizes the free energy at a given interfacial area in the presence of surplus water (and oil).

Phase-separation kinetics

Driving a mixture into the 2Φ region by constantly heating leads to a periodic clouding and clearing of the mixture [21, 22, 36]. The succession of cloudings is due to strong threshold behavior in the formation of aggregates (in this case water droplets) larger than the wavelength of light. The change in the turbidity can, however, only be investigated optically when the turbidity changes significantly during an oscillation [21]. Due to a small signal-to-noise level only two to four cloudings can be discerned optically for most compositions and heating rates.

More detailed information about the kinetics of this phase separation can be achieved from microcalorimetric measurements [21]. In contrast to optical measurements, which are sensitive to large particles in the system, the specific heat is sensitive to changes in the curvature of the interface [19]; thus, it is affected by all droplets and governed, in particular, by the vast majority of small ones. For that reason, the values for the apparent specific heat contain less noise and even give an oscillating signal when nothing can be discerned any longer in the optical data. The microcalorimetric data allow the oscillations to be investigated quantitatively. The measurements were performed with a MicroCal VP-DSC differential scanning microcalorimeter (Northhampton, Mass., USA). It consists of twin, coin-shaped, fixed-in-place cells each of 0.5 ml, mounted in an adiabatic chamber. Accuracies of about 50 μJ K^{-1} cm^{-3} for $C_v^{rel}(T)$ are achieved.

The temperature-dependent variation for the signal of the apparent specific heat $C_v^{rel}(T)$ is shown in Fig. 3 for different heating rates. For all heating rates about 15 oscillations are discerned. The period, or the time lag, ΔT, between two succeeding maxima increases with increasing v_s. Previously, we showed that $\Delta T \propto \sqrt{v_s}$ [21, 23]. For a definition of ΔT and the height of the peak $\Delta C_v(T)$ see the inset of Fig. 3.

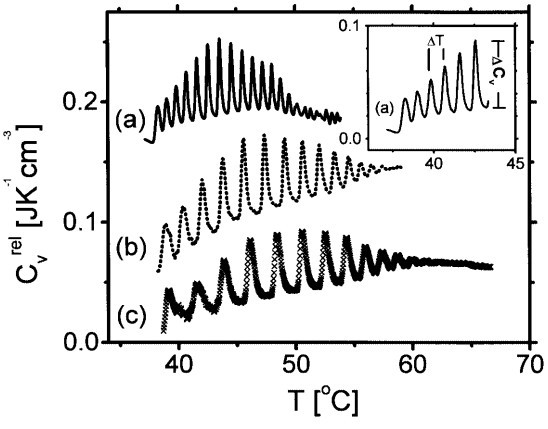

Fig. 3 Temperature-dependent variation of the apparent signal for the specific heat, $C_v^{rel}(T)$, while entering the $\overline{2\Phi}$ region with three different heating rates: (*a*) $v_s = 4$ K/h, *solid line*; (*b*) $v_s = 14$ K/h, *dotted line*; (*c*) $v_s = 27$ K/h, *crosses*. To avoid crossings, the data for the apparent specific heat are shifted vertically. The sample composition is given by $\phi_s = 0.1$, $\phi_w = 0.33$, and $\phi_o = 0.57$. The *inset* shows the definition of the height of a peak, i.e., of ΔC_v, and of the period of an oscillation, ΔT

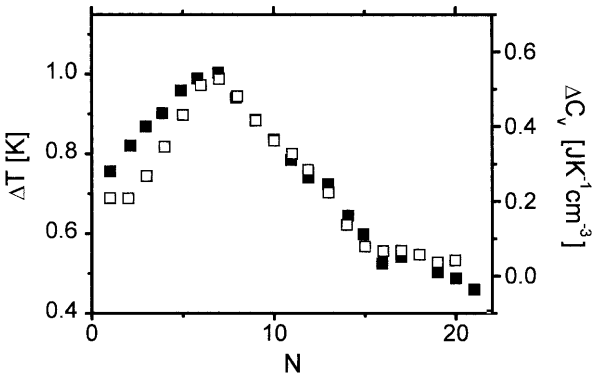

Fig. 4 Dependence of the time lag between two succeeding maxima, ΔT, and of the height of a peak, ΔC_v, on the number of oscillations N ($\phi_s = 0.1, \phi_w = 0.33, v_s = 4\mathrm{K/h}$)

Both, ΔT and ΔC_v change nonmonotonously with the number of oscillations, i.e., with the temperature. These dependencies become evident when the signal for the apparent specific heat shows a pronounced superimposed structure. The close connection between ΔT and ΔC_v is supported by the similarity of the variation of $\Delta T(N)$ (Fig. 4: filled squares, left axis) and $\Delta C_v(N)$ (Fig. 4: open squares, right axis) with N. Both $\Delta T(N)$ and $\Delta C_v(N)$ first increase with the number of oscillations, pass a maximum, and eventually decrease for large values of N.

Mechanism of phase separation and energy barrier

Mechanism of phase separation

To understand the origin and the parameter dependence of the kinetics we first discuss the mechanism of phase separation. Figure 1 gives a schematic view of the microstructure within a small volume element, $\tilde{V}$, at different temperatures, with constant heating of the mixture. At the WEB, $T \approx T_{\mathrm{WEB}}$ (Fig. 1a), the mixture is a single phase and consists of N nearly monodisperse droplets of radius R. If the mixture were heated above the WEB droplets want to decrease in size; however, this is not easy since the mixture has to conserve its total surface area and volume of water and surfactant. Assuming that exchange of surfactant and water by diffusion through octane is negligible on the experimental time scale, the droplets can only exchange water and surfactant by collisions[2]. Therefore, the size of the droplets does not change (cf. Fig. 1b) even though the droplets are supersaturated after some heating. Only when strongly overheating the mixture may a single large droplet be formed within the volume element, $\tilde{V}$, taking away the surplus water (Fig. 1c). Note, that the formation and growth of droplets larger than the optimum size is always energetically disfavorable for single droplets; however, large droplets may be formed, allowing the majority of small droplets to attain their optimum size. As a large droplet is energetically "expensive" the droplets need to pass an energy barrier before moving closer to the equilibrium state. As soon as the large droplet exists it will grow by taking up excess water of the small droplets and will merge with larger droplets until it finally sediments and merges with the water-rich phase (Fig. 1d).

Energy barrier

The height of the energy barrier can be calculated as the maximum value of the difference (ΔF_b) of the free energy, $F_b(N,R)$, of the supersaturated state (see Fig. 1b) and of $F_b(N',R') + F_b(1,\rho)$ describing the final state (Fig. 1c), where N' particles of radius $R'(R > R' \gtrsim R_{\mathrm{opt}})$ coexist with a single large droplet of radius ρ [22]:

$$\Delta F_b = F_b(N',R') + F_b(1,\rho) - F_b(N,R) \ . \qquad (4)$$

As soon as $\Delta F_b < 0$, it is energetically favorable to form N' droplets of radius R' and a single big droplet of radius ρ. The dependence of ΔF_b on the reduced size of the large droplet, $(\rho - R)/\rho$, is shown in Fig. 5 for $N = 1000$ for different amounts of overheating, $\tau \equiv R/R_{\mathrm{opt}} \propto (T - \overline{T})$. The monodisperse state corresponds to $(\rho - R)/\rho = 0$, whereas $(\rho - R)/\rho \to 1$ if $\rho \gg R$. For small values of $\tau(\tau = 1.1)$ ΔF_b always increases with increasing reduced size of the large droplet. The

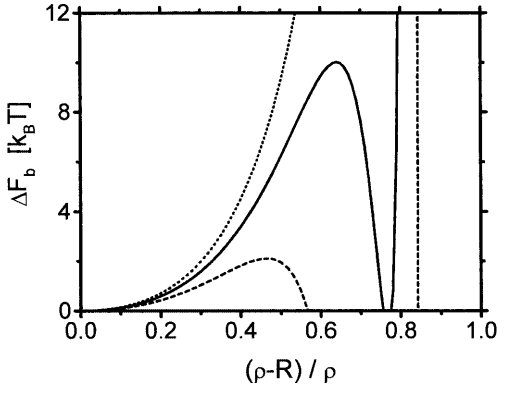

Fig. 5 Dependence of the energy difference of the initial and final states, ΔF_b, as a function of the reduced size of a large excess droplet, i.e., $(\rho - R)/\rho$, for different degrees of overheating and fixed $N = 1000$. *Dotted line*: $\tau = 1.1$; *solid line*: $\tau = 1.15$; *dashed line*: $\tau = 1.22$

[2] In contrast to this, Olsson, Wennerström and coworkers expect that the dominant mechanism for mass transport is molecular diffusion of alkane and surfactant through water for the phase separation of oil droplets in water into an oil-rich phase coexisting with oil droplets [9, 10]. We do not see, however, how to explain the parameter dependence of the superimposed structure in the signal for the apparent specific heat by a molecular diffusion mechanism (see later)

monodisperse system is stable. On increasing the overheating a second minimum shows up. Only for $\tau \approx 1.15$ does the energy difference become negative when a sufficiently large excess droplet is formed; however, the mixture has to pass an energy barrier, ΔF_b^{max}, of the order of $10 k_B T$. ΔF_b^{max} decreases towards a few $k_B T$ for $\tau = 1.22$ and ΔF_b becomes negative for $(\rho - R)/\rho \approx 0.55$, i.e., for $\rho \approx 2R$.

The dependence of the height of the energy barrier, ΔF_b^{max}, on the reduced temperature τ, i.e., on $R/R_{opt}(T)$, is shown in Fig. 6. The solid line corresponds to the case when $N = \infty$ droplets participate in forming the large droplet. As shown in Fig. 6, the height of the barrier decreases rapidly with increasing overheating. For $R \approx 1.2\, R_{opt}$ it has decreased towards a few $k_B T$ from the diverging value taken at $R = R_{opt}$.

The dotted lines show the influence of the number of droplets on ΔF_b^{max}. For every finite value of N, the dotted lines terminate for a given degree of overheating. The minimum degree of overheating increases with decreasing N. If the mixture is overheated below this N-dependent minimum value, the droplets expel too little water to build a sufficiently large droplet in order for ΔF_b to become negative (Fig. 5); however, once the formation of a large droplet becomes possible, i.e., $\Delta F_b < 0$, the height of the energy barrier depends only slightly on N. Note, that energy barriers of a few $k_B T$ require values for $R/R_{opt} \approx 1.2$ in accordance with experimental observations [22]. This implies that at least a few hundred droplets participate in forming a single large droplet, implying that the nucleation of large water droplets is a strongly collective process.

Model for cascade nucleation

We now further discuss Fig. 1 in order to clarify the origin of cascade nucleation in more detail (see also Refs. [22, 23]). To this end we observe that for low supersaturation (Fig. 1b, $\tau \lesssim 1.15$) nucleation is strongly suppressed for energetic and kinetic reasons, while it becomes very fast for larger values of τ, leading locally to a structure as shown in Fig. 1c. Typically, a large droplet is nucleated by at most every few thousand small ones, such that in a very short time a macroscopic number of nuclei (above about 10^{14}) appear in the sample. They are homogeneously distributed with typical distances below a few hundred nanometers such that they induce a rapid relaxation of the droplet size distribution to a close-to-equilibrium state. At the same time the nuclei grow in size and merge into water-rich domains, whose mutual distance soon exceeds 10–100 μm. By that time a typical neighborhood of a water-rich domain contains a few thousand small droplets and it looks very much the same as those sketched in Fig. 1a. Due to the large distance between the water-rich domains and the majority of small droplets, water transport – no matter whether by molecular diffusion of water through the oil or by diffusion and collisions of droplets – from small droplets to the water-rich domains is negligible on the time scales of the experimental heating rates. Consequently, the droplets cannot change their size upon heating, again leading to supersaturation (Fig. 1b) and eventually to nucleation (Fig. 1c), but now for droplets with a slightly changed radius and density. This is hinted at in Fig. 1 by the arrow pointing back from pictures c and d to picture a. We conclude, that the stepwise decrease in the droplet size was due to alternation between long periods of slow heating and comparatively rapid relaxation after nucleation arose in the system. Hence, cascade nucleation involves at least two, typically quite different time scales:

1. The times scale $t_1 \propto (a R_{opt} v_s)^{-1}$ characterizes the change in the optimum droplet radii due to heating.
2. The time scale t_2 is set by the inverse of the decay rate, γ, of the number of big droplets in the system due to coalescence, where the probability for coalescence depends on the distance between large droplets, D_{big}, and their diffusion speed, $\mathscr{D}_{diff}$, as $t_2^{-1} \propto \gamma \propto \mathscr{D}_{diff}/D_{big}^2$.

For a theoretical discussion of this picture from a more general point of view, we refer to Ref. [23]. Here, we only remark that the bottom line of the arguments presented in Ref. [23], is that the time $\Delta T/v_s$ between subsequent bursts of nucleation scales as the geometric mean of the time scales t_1 and t_2, leading to

$$\left(\frac{v_s}{\Delta T}\right)^2 = \frac{1}{t_1\, t_2} \propto a R_{opt} v_s\, \frac{\mathscr{D}_{diff}}{D_{big}^2} \quad . \tag{5}$$

Moreover, the distance D_{big} between large droplets can be related to the composition of the microemulsion by equating D_{big}^3 to the volume occupied by N small droplets in the region of the sample containing only a single large droplet,

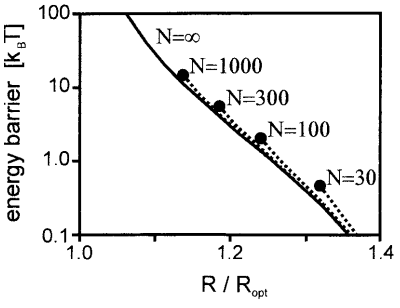

Fig. 6 The *line* indicates the height of the energy barrier ΔF_b^{max} for $N = \infty$ as a function of the reduced temperature R/R_{opt}. The *dotted lines* terminated by *dots* show numerical solutions for the energy barrier for different finite values of N

$$D_{\mathrm{big}}^3 = \frac{4\pi}{3} N \frac{R_{\mathrm{opt}}^3}{\phi_{\mathrm{d}}} \quad . \tag{6}$$

Combining Eqs. (5) and (6) leads to the prediction

$$\Delta T^2 \sim \frac{R_{\mathrm{opt}}}{\phi_{\mathrm{d}}^{2/3}} v_{\mathrm{s}} \quad , \tag{7}$$

provided one assumes that $\mathscr{D}_{\mathrm{diff}}$ and N can be considered constant. For the first oscillations after crossing the WEB the radius of the droplets is still very close to its value in the 1Φ region, $R_{\mathrm{opt}} \approx R_{1\phi}$. In this situation, the prediction of Eq. (7) agrees remarkably well with the experimental data, as demonstrated in Fig. 7. When plotting ΔT against $R_{1\Phi} v_{\mathrm{s}} \phi_{\mathrm{d}}^{-2/3}$ on a log-log scale, the data for a variety of compositions and scan speeds collapse onto a single line with slope 0.5, as predicted by Eq. (7).

Temperature-dependent droplet–droplet distance

The dependence of ΔT^2 on $v_{\mathrm{s}} R_{1\phi} \phi_{\mathrm{d}}^{-2/3}$ has been verified for the first oscillations. This is not sufficient to explain the dependence of ΔT on the number of oscillations, which has been observed when the specific heat shows a pronounced superimposed structure (Fig. 3).

To understand this dependence, the implications of volume and surface conservation on the number of droplets and on the average droplet–droplet distance, $D_{\mathrm{d-d}}$ have to be considered. According to Eq. (2) the optimum size of the droplets decreases with increasing temperature. This implies that the volume fraction of the droplets also decreases (equating Eqs. 1 and 2),

$$\phi_{\mathrm{d}} = \frac{\phi_{\mathrm{s}}}{3 l_{\mathrm{s}}} R_{\mathrm{opt}} \quad , \tag{8}$$

whereas the number density, n, of droplets increases

$$n \equiv \frac{N}{V} = \frac{\phi_{\mathrm{s}}}{4\pi l_{\mathrm{s}} R_{\mathrm{opt}}^2} \tag{9}$$

The change in the optimum radius, and correspondingly in $D_{\mathrm{d-d}}$, upon increasing temperature is shown schematically in Fig. 8. (The relation of the size of the droplets is chosen to reflect the situations at the beginning and the end of a typical experiment.) In Fig. 8a a droplet configuration is given as it may exist at the WEB $T_1 = T_{\mathrm{WEB}}$. The droplets take their optimum radius $R_{\mathrm{opt}}(T_1) = R_{1\Phi}$; $D(T_1)$ denotes the average distance between droplet interfaces. In Fig. 8b, at $T = T_2$, the mixture is deep in the 2Φ region. The size of the droplets has decreased towards $R_{\mathrm{opt}}(T_2)$ and, correspondingly, the average droplet–droplet distance has decreased towards $D_{\mathrm{d-d}}(T_2)$. Due to conservation of the total interfacial area and of the volume fraction of all components the number of droplets increased. The excess water which could no longer be dissolved in the smaller-sized droplets has been expelled into a water-rich phase formed at the bottom of the test tube.

The average droplet–droplet distance can be calculated, assuming locally a close-packed arrangement of droplets

$$D_{\mathrm{d-d}} \simeq \frac{1}{\sqrt{2}} \left(\frac{16\pi}{3} \right)^{1/3} \frac{R_{\mathrm{opt}}(T)}{\phi_{\mathrm{d}}^{1/3}} \tag{10a}$$

$$\propto \frac{R_{\mathrm{opt}}^{2/3}}{\phi_{\mathrm{s}}^{1/3}} \quad . \tag{10b}$$

$D_{\mathrm{d-d}}$ decreases with increasing temperature and surfactant concentration. For the collision frequency, however, not the average droplet–droplet distance, but the average distance, D, between the interfaces between neighboring droplets is relevant.

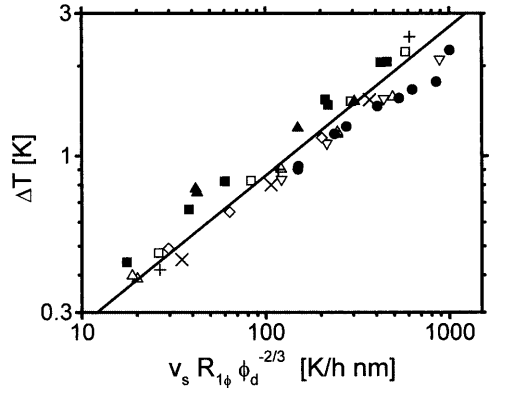

Fig. 7 Composition dependence of the square of the period of the first oscillation ΔT^2 on $v_{\mathrm{s}} R_{1\phi} \phi_{\mathrm{d}}^{2/3}$. The *symbols* show the results of microcalorimetric measurements on nine different compositions with typically three different heating rates per sample. The *straight line* is a fit through the data points with slope 0.5. Sample compositions: $\phi_{\mathrm{d}} = 0.096, R = 5.8$ nm (▽); $\phi_{\mathrm{d}} = 0.094, R = 16$ nm (+); $\phi_{\mathrm{d}} = 0.19$, $R = 5.8$ nm (△); $\phi_{\mathrm{d}} = 0.19$, $R = 6.8$ nm (●); $\phi_{\mathrm{d}} = 0.19$, $R = 15$ nm (◇); $\phi_{\mathrm{d}} = 0.38$, $R = 6.0$ nm (▲); $\phi_{\mathrm{d}} = 0.37$, $R = 8.2$ nm (■); $\phi_{\mathrm{d}} = 0.38$, $R = 11$ nm (□); $\phi_{\mathrm{d}} = 0.38$, $R = 15$ nm (×)

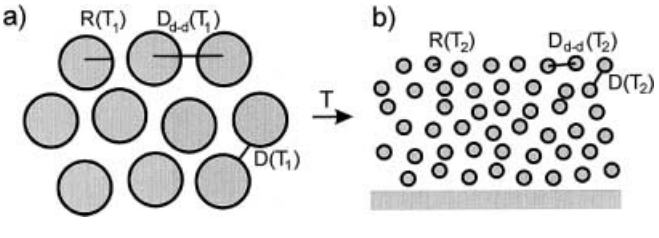

Fig. 8 Schematic drawing of the radius of the droplets, R, the average droplet–droplet distance, $D_{\mathrm{d-d}}$, and the average distance between droplet boundaries, D, for two temperatures. At $T_1 = T_{\mathrm{WEB}}$ the mixture is a single phase; $R_{1\Phi} = R_{\mathrm{opt}}(T_1) \equiv R(T_1)$. At $T = T_2$ the mixture consists of two phases; $R_{\mathrm{opt}}(T_2) \equiv R(T_2)$. The water not emulsified by the droplets is expelled into a coexisting water-rich phase

$$D \equiv D_{\mathrm{d-d}}(T) - 2R_{\mathrm{opt}}(T) \tag{11a}$$

$$\simeq 2(l_{\mathrm{s}}R_{\mathrm{opt}}^2)^{1/3}\left[\frac{1}{\sqrt{2}}\left(\frac{2\pi}{\phi_{\mathrm{s}}}\right)^{1/3} - \left(\frac{R_{\mathrm{opt}}}{l_{\mathrm{s}}}\right)^{1/3}\right] . \tag{11b}$$

The temperature dependence of $D_{\mathrm{d-d}}(T)$ is compared to the temperature dependence of $D(T)$ in Fig. 9. Note, that $D(T)$ varies non-monotonically with temperature. First, $D(T)$ increases with increasing temperature, then it passes a maximum at $T = T_{\mathrm{m}}$, and eventually it decreases with increasing temperature. The data points indicate the corresponding temperatures of the peaks in the measurements for the apparent specific heat (cf. Fig. 3a for the raw data for $C_v^{\mathrm{rel}}(T)$ and Fig. 4 for the dependence of ΔT and ΔC_v on N). The nonmonotonic temperature dependence of $D(T)$ can be understood from the interplay of the decrease in $R_{\mathrm{opt}}(T)$ with increasing temperature and the increase in the number of droplets leading to a decrease in $D_{\mathrm{d-d}}(T)$. For $T < T_{\mathrm{m}}$ the increase in D results from a faster decrease in $R_{\mathrm{opt}}(T)$ than the decrease in $D_{\mathrm{d-d}}(T)$. For $T > T_{\mathrm{m}}$ the decrease in $D_{\mathrm{d-d}}(T)$ due to the increase in the number of droplets dominates the decrease in the size of the droplets, leading to a decrease in $D(T)$.

Figure 10 shows the N dependence of $\Delta T D^{-2} v_{\mathrm{s}}^{-1/2}$, where N is a measure for the temperature. The different symbols denote different heating rates, while the composition of the mixture is kept equal: $\phi_{\mathrm{s}} = 0.1$ and $\phi_{\mathrm{w}} = 0.33$. To achieve the data collapse the dependence of ΔT on $\sqrt{v_{\mathrm{s}}}$ [21, 23] is taken into account. Within the error margin the data for $\Delta T D^{-2} v_{\mathrm{s}}^{-1/2}$ do not depend on N any longer. The slight decrease in $\Delta T D^{-2} v_{\mathrm{s}}^{-1/2}$ on increasing the heating rate may be due to different entracement of oil and surfactant into the water-rich phase. This additional change of composition (on top of the expelling of water) is more pronounced for high

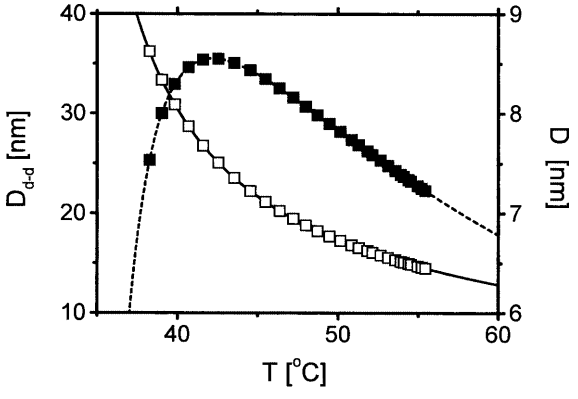

Fig. 9 The dependences of $D_{\mathrm{d-d}}$ (*left axis*, *solid line*) and D (*right axis*, *dashed line*) as functions of temperature for $\phi_{\mathrm{s}} = 0.1$. $D_{\mathrm{d-d}}$ decreases with increasing temperature, whereas D shows a nonmonotonic temperature dependence. The *data points* denote the values for the peaks observed in the measurements of the apparent specific heat (cf. the curve for $\phi_{\mathrm{s}} = 0.1$ and $v_{\mathrm{s}} = 4$ K/h in Fig. 3)

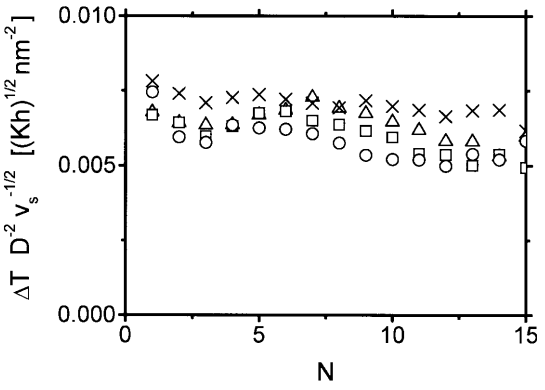

Fig. 10 Dependence of $\Delta T D^{-2} v_{\mathrm{s}}^{-1/2}$ on the number of oscillations, N, for $\phi_{\mathrm{s}} = 0.1$ and $\phi_{\mathrm{w}} = 0.33$. The *data points* correspond to four different scan speeds: $v_{\mathrm{s}} = 1.2$ K/h (×); $v_{\mathrm{s}} = 4$ K/h (△); $v_{\mathrm{s}} = 13$ K/h (□), $v_{\mathrm{s}} = 27$ K/h (○)

heating rates, because in that case the water-rich phase has less time to relax towards a close-to-equilibrium state, leading to more significant changes of composition within the microemulsion phase. In any case, however, the independence of $\Delta T D^{-2}$ on N indicates that the observed dependence of ΔT on N is due to the change in the droplet–droplet distance with N. The square dependence on D supports our assumption that mass transport is via diffusion of the nanometer-sized microemulsion droplets.

Conclusion

We have presented a model for cascade nucleation in the phase separation of a droplet phase microemulsion driven across the emulsification boundary by constant heating. Beyond this phase boundary the droplets tend to shrink, leading to the formation of a coexisting water-rich phase; however, due to conservation of the overall surface area of the droplets and of the volume fraction of all components, nuclei can only be formed collectively by a large number of individual droplets. The height of the energy barrier shrinks with the degree of overheating. After having passed the energy barrier the majority of microemulsion droplets rapidly shrink at the expense of a few nuclei. The nuclei grow rapidly by taking up the excess water. At the same time their number decreases due to coalescence and sedimentation. The switching between slowly increasing supersaturation due to heating and fast relaxation at strong supersaturation appears to be the origin of cascade nucleation.

The experimental data suggest that the time lag between bursts of nucleation depends on $\sqrt{v_{\mathrm{s}}}$. This dependence not only holds for the whole range of compositions, but remains valid during the whole phase-separation process. The variation of ΔT with the number of oscillations, or temperature, is found to be properly

described by the temperature-dependent change of the average distance between the respective surface of neighboring droplets. D varies nonmonotonically with temperature due to the interplay of a temperature, induced decrease in the size of the droplets and an increase in the number of droplets due to conservation of the total interfacial area. The negligible dependence of $\Delta T D^{-2}$ on N supports our assumption that interfacial area is conserved although the system is far from equilibrium and that mass transport is dominated by droplet diffusion.

In conclusion, we would like to stress the deterministic behavior of the kinetics of this temperature-driven phase separation. Although the system is heated for several hours and is deep in the 2Φ region, the energy barrier preventing nucleation and the period of the oscillations can be described only by taking into account the temperature dependence of the preferred curvature of the surfactant monolayer, conservation of total interfacial area and of the volume fraction of all compounents, and a separation of time scales. It might be expected that these parameters are also crucial to describe the kinetics of surfactant mixtures for systems driven out of equilibrium by other mechanisms.

Acknowledgements It is a pleasure to thank M. Schmidt for support in performing this work and R. Strey and J. Vollmer for fruitful and pleasant collaboration. The latter also carefully read the manuscript. Support of the Deutsche Forschungsgemeinschaft is acknowledged.

References

1. Diat O, Roux D, Nallet F (1993) J Phys II 3:1427
2. Diat O, Roux D, Nallet F (1995) Phys Rev E 59:3296
3. Bergmeier M, Hoffmann H, Thunig C (1997) J Phys Chem B 101:5767
4. Arrault J, Grand C, Poon W, Cates ME (1997) Europhys Lett 38:625
5. Buchanan M, Arrault J, Cates ME (1998) Langmuir 14:7371
6. Mishima K, Yoshiyama K (1987) Biochim Biophys Acta 904:149
7. Sakurai I, Suzuki T, Sakurai S (1989) Biochim Biophys Acta 985:101
8. Miller CA, Raney KH (1993) Colloids Surf A 74:169
9. Morris J, Olsson U, Wennerström H (1997) Langmuir 13:606
10. Wennerström H, Morris J, Olsson U (1997) Langmuir 13:6972
11. Kabalnov A, Weers J (1996) Langmuir 12:1931
12. Goldstein RE, Nelson P, Powers T, Seifert U (1996) J Phys II 6:767
13. Safran SA, Turkevich LA, Pincus P (1984) J Phys Lett 43:2903
14. Safinya CR, Sirota EB, Roux D, Smith GS (1989) Phys Rev Lett 62:1134
15. Andelman D, Cates ME, Roux D, Safran SA (1987) J Chem Phys 87:7229
16. Olsson U, Wennerström H (1994) Adv Colloid Interface Sci 49:113
17. Strey R (1994) Colloid Polym Sci 272:1005
18. Sicoli F, Langevin D, Lee LT (1993) J Chem Phys 99:4759
19. Vollmer D, Strey R (1995) Europhys Lett 32:693
20. Sottmann T, Strey R (1997) J Chem Phys 106:8605
21. Vollmer D, Strey R, Vollmer J (1997) J Chem Phys 107:3619
22. Vollmer J, Vollmer D, Strey R (1997) J Chem Phys 107:3627
23. Vollmer J, Vollmer D (1999) Faraday Discuss 112:51
24. Langevin D, Meunier J (1994) In: Gelbart WM, Ben-Shaul A, Roux D (eds) Micelles, membranes, microemulsions, and monolayers. Springer, Berlin Heidelberg New York, pp 485–519
25. M. Kahlweit M, Strey R, Busse G (1990) J Phys Chem 94:3881
26. Strey R, Glatter O, Schubert K-V, Kaler EW (1996) J Chem Phys 105:1175
27. Gompper G, Schick M (1994) In: Domb C, Lebowitz JL (eds) Phase transitions and critical phenomena vol 16. Academic Press London, pp 1–175
28. Kahlweit M, Strey R (1985) Angew Chem Int Ed Engl 24:654
29. Kahlweit M, Strey R, Busse G (1993) Phys Rev E 47:4197
30. Kahlweit M, Strey R, Firman P (1986) J Phys Chem 90:671
31. Vollmer D, Vollmer J, Strey R (1996) Phys Rev E 54:3028
32. Bagger-Jörgensen H, Olsson U, Mortensen K (1997) Langmuir 13:1413
33. Clark S, Fletcher PDI, Ye X (1990) Langmuir 6:1301
34. Safran SA, Turkevich LA (1983) Phys Rev Lett 50:1930
35. Helfrich W (1973) Z Naturforsch C 28:693
36. Vollmer D, Vollmer J, Strey R (1997) Europhys Lett 39:245